FRONTIERS OF PHYSICS

RESEARCH ARTICLE
Volume 18 / Issue 3 / 33306 / 2023

Excited state biexcitons in monolayer WSe_2 driven by vertically grown graphene nanosheets with high-density electron trapping edges

Bo Wen[1,*], Da-Ning Luo[1,*], Ling-Long Zhang[1,2,*], Xiao-Lin Li[1], Xin Wang[3], Liang-Liang Huang[1], Xi Zhang[1,†], Dong-Feng Diao[1]

1 Institute of Nanosurface Science and Engineering Guangdong Provincial Key Laboratory of Micro/Nano Optomechatronics Engineering, Shenzhen University, Shenzhen 518060, China
2 College of Physics, Nanjing University of Aeronautics and Astronautics, Key Laboratory of Aerospace Information Materials and Physics (NUAA), MIIT, Nanjing 211106, China
3 Research Center of Medical Plasma Technology, Shenzhen University, Shenzhen 518060, China
Corresponding author. E-mail: †zh0005xi@szu.edu.cn
*These authors contributed equally to this work.
Received October 17, 2022; accepted November 23, 2022

ABSTRACT

Interface engineering in atomically thin transition metal dichalcogenides (TMDs) is becoming an important and powerful technique to alter their properties, enabling new optoelectronic applications and quantum devices. Interface engineering in a monolayer WSe_2 sample via introduction of high-density edges of standing structured graphene nanosheets (GNs) is realized. A strong photoluminescence (PL) emission peak from intravalley and intervalley trions at about 750 nm is observed at the room temperature, which indicated the heavily p-type doping of the monolayer WSe_2/thin graphene nanosheet-embedded carbon (TGNEC) film heterostructure. We also successfully triggered the emission of biexcitons (excited state biexciton) in a monolayer WSe_2, via the electron trapping centers of edge quantum wells of a TGNEC film. The PL emission of a monolayer WSe_2/GNEC film is quenched by capturing the photoexcited electrons to reduce the electron-hole recombination rate. This study can be an important benchmark for the extensive understanding of light–matter interaction in TMDs, and their dynamics.

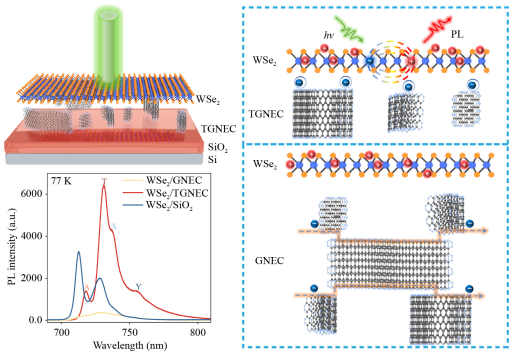

Keywords excited state biexcitons, monolayer WSe_2, vertically graphene, electron trapping edges

1 Introduction

Since the isolation of graphene, which has led to a boom in the study of two-dimensional materials [1]. The special structure of two-dimensional materials results in unique electrical, optical and mechanical properties [2–4]. After a thorough study of graphene materials and their devices, it was found that the zero band gap property of graphene greatly limits its application in electronic and optical devices. In the case of two-dimensional transition

#Special Topic: Two-dimensional Electronic Materials and Devices (Eds.: Lin Wang & Xiaolong Chen).

https://doi.org/10.1007/s11467-022-1232-8

metal dichalcogenides (TMDs), such as MoS_2, $MoSe_2$, WS_2 and WSe_2, the energy band structure changes as the number of layers decreases; the band gap changes from a blocky indirect band gap to a direct band gap in a single thin film; and the optical, electrical and mechanical properties also change significantly [5–8]. TMDs can interact directly and strongly with light, with a band gap covering the near-infrared to visible wavelengths, and have promising applications in optoelectronic devices [9–11]. However, the conductivity of TMDs is low [12], and by introducing various highly conductive materials (e.g., carbon materials, MXenes) as conductive networks for compounding with TMDs [13–18]; the interface modulation between conductive networks and TMDs is achieved to fully utilize the advantages of composites [19, 20].

In low-dimensional TMDs materials, the Coulomb interaction in these atomic thin layers is highly enhanced due to the reduced dimensionality and weak dielectric shielding [21]; the ground-state electrons in two-dimensional TMDs materials are excited to jump to the conduction band with valence band holes in Coulomb interaction, form tightly bound excitons (a bound state of one electron and one hole) [22]，trions (a bound state of an exciton plus an additional electron or hole) [23, 24], and biexcitons (a bound state of double excitons) [25, 26]. These excitonic complexes have a large binding energy between a few hundred millivolts, and these values are more than an order of magnitude larger than that in conventional III-V-based quasi-2D semiconductor quantum wells (QWs), so they can be easily observed at room temperature and the photoresponse of TMDs is dominated by these excitons [27–32].

In this work, we introduced edge quantum wells (QWs) as electron capture centers through vertical graphene nanosheet-embedded carbon (GNEC) films, and explored the photoluminescence (PL) capability of carbon films combined with monolayer WSe_2. In order to study the effect of carbon film on the exciton state in monolayer WSe_2, the thin and thick carbon films were manufactured separately for comparison. We also performed photoluminescence measurements related to the incident power to confirm the emission properties of different exciton states, which show a linear increase with increasing excitation power at different slopes. Photoluminescence at different temperatures was also tested to explore the thermal stability of excitons in different bound states with increasing temperature. The geometric limit of monolayer TMDs causes enhanced Coulomb interactions and modulates the many-body exciton state of monolayer TMDs materials through edge traps of graphene carbon films, which can govern the optical properties and carrier transport properties. A microscopic understanding of how excitons are formed from other carriers is essential for elucidating the potential physical mechanism of many-body interactions in TMDs materials as well as for applications in optoelectronic devices.

2 Methods

GNEC film deposition and characterization.

Monolayer WSe_2 samples were produced by (CVD). Then, monolayer WSe_2 chip was wet-transferred onto a SiO_2/Si substrate (280 nm thermal oxide on n^+-doped silicon), with half on a GNEC film and half on a TGNEC film. The GNEC film was deposition by ECR process. The thickness of GNEC film is about 70 nm. A polyimide (PI) film was used as an isolation layer to deposit thin GNEC film. The nanostructures of the carbon films were analyzed by TEM (FEI, Titan3 Themis G2) and AFM (Dimension ICON).

Optical characterization. Raman and PL measurements were conducted using a Horiba LabRAM system equipped with a confocal microscope, a charge-coupled device (CCD) Si detector, and a 532 nm diode-pumped solid-state laser as the excitation source. The laser light was focused on the sample surface via a 50× objective lens (Olympus, LMPLFLN50X). The spectral response of the entire system was determined with a calibrated halogen–tungsten light source. The PL signal was collected by a grating spectrometer, thereby recording the PL spectrum through the CCD (Princeton Instruments, PIXIS). All the PL spectra were corrected for the instrument response. For temperature-dependent measurements, WSe_2/GNEC film chips were put into a Linkam THMS 600 chamber and the temperature was set to a constant (range from 298 to 77 K) during the PL measurements using a low-temperature controller with liquid nitrogen coolant.

3 Results and discussion

Vertical graphene nanosheet-embedded carbon (GNEC) films were made using an electron cyclotron resonance (ECR) plasma sputtering system. The ECR plasma sputtering system has been described in detail in our previous work [33–35]. The involvement of low-energy electrons leads to the vertical growth of graphene nanocrystals embedded in amorphous carbon on the substrate. Microwaves with power of 500W are used in the vacuum chamber, followed by plasma generation at an argon pressure of 4×10^{-2} Pa. By applying a symmetrically confined magnetic field to the system to increase the plasma density, the negatively biased carbon target is sputtered by high-speed bombardment of Ar^+ ions, and the carbon atoms separated by the bombardment move toward the substrate. In the deposition manufacturing process, we divide the SiO_2/Si substrate into two equal areas. Polyimide (PI) film is applied on one side and the other side is left untreated. PI polymer

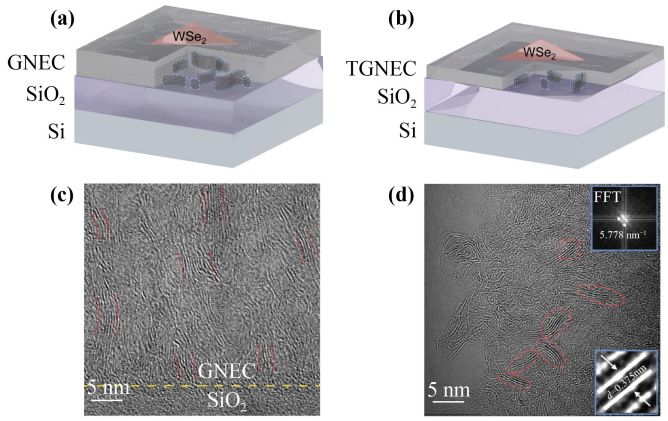

Fig. 1 **(a)** Structural model of vertical graphene nanosheet-embedded (GNEC) film. **(b)** Structural model of vertical thin graphene nanosheet-embedded (TGNEC) film. **(c)** High-resolution TEM micrographs of 80 V GNEC film cross-section sample. **(d)** Top-view TEM images of carbon films. Insets show the FFT images and the crystal plane spacing.

film plays a filtering and screening role, carbon atoms will be deposited on the silicon substrate through the polymer film to form a thin graphene nanosheet-embedded carbon (TGNEC) film [Fig. 1(b)], and the other side without treatment will be deposited as a thicker GNEC film [Fig. 1(a)]. Deposition time is set to 30 minutes at a bias voltage of 80 V.

The graphene nanosheets in the thick GNEC film are rich in content [Fig. 1(a)], diverse in morphology and dense, and easy to form a conductive network, with excellent carrier conduction ability. The thin GNEC film contains few graphene nanosheets [Fig. 1(b)], which are scattered and almost non-conductive, and the high density of the edges will capture electrons, which will easily make the monolayer WSe_2 giving rise to excitonic complexes and enhance the photoluminescence of the device. The surface characteristics of GNEC were observed by using transmission electron microscope (TEM). We can clearly observe the presence of graphene nanocrystals from the cross-section [Fig. 1(c)] and the top view [Fig. 1(d)] surface of the carbon film. In addition, the Laue spots are clearly observed from the FFT image of GNEC; the reciprocal lattice distance between the two spots is 5.778 nm^{-1}; the crystal plane spacing in this direction is calculated to be $d = 0.375$ nm; corresponding to the (0001) plane of multilayer graphene, indicating that the nanocrystal is multilayer graphene [36, 37].

WSe_2 samples grown by chemical vapor deposition (CVD) were wet-transferred onto SiO_2/Si wafers with two different thicknesses of carbon films deposited. WSe_2 is n-doping induced by defect engineering and contains a large number of free electrons inside, which greatly improves its conductivity [16]. The same WSe_2 samples were also transferred on the SiO_2/Si substrate without carbon film growth as a control reference. The PL spectra of the samples were then measured, and the WSe_2-GNEC samples were kept in a Linkam microscopy-compatible cryostat at 25 °C during the measurements. The liquid nitrogen flows continuously to maintain the low temperature during the tests. The single-layer WSe_2 combined with thick GNEC film emits light weakly [Fig. 2(a)]. Due to the high content of graphene nanocrystals in the thick carbon film, it is prone to form a conductive network [Fig. 2b]. The photogenerated carriers flow away in direct conduction and are not easily formed into emitted photons. The photoluminescence of the WSe_2 sample coupled with a thin carbon film (WSe_2/TGNEC) is significantly stronger than that of the monolayer WSe_2 on SiO_2 [Fig. 2(c)]. There are four different peaks at wavelengths of 720 nm, 730 nm, 735 nm and 755 nm [Fig. 2(c)], respectively designated as A, T, X and Y peaks. In the following study, we will confirm which exciton complexes are responsible for these characteristic peaks. The highest peak is at 730 nm, which is much larger than the highest peak in conventional WSe_2, and the A peak is decreased compared to conventional monolayer WSe_2. The reason for the different peaks in the WSe_2/TGNEC is the formation of edge quantum wells (QWs) at the high-density edges of GNEC film [Fig. 2(b)] [38], where a large number of electrons are concentrated. The optical response of WSe_2 is also dominated by excitons. We also tested the luminescence ability of different WSe_2 samples, and the highest peak was found to be basically stable at around 745 nm with stable luminescence performance in multiple measurements. The monolayer WSe_2 is heavily p-type doping containing a large number of holes, which combine with photoexcited leaping electrons to form tightly bound excitons, trions and biexcitons. When the energy of the photon is sufficient to excite the electron from the valence band to the conduction band, the photon is absorbed in the semiconductor or insulator. Photoluminescence is simply an opposite process in which electrons in the conduction band recombine with holes in the valence band under the emission of photons. Strong Coulomb interactions due to less charge shielding form special excitonic complexes with large binding energies that remain stable even at room temperature [39–41]. At low temperatures, the emission of bound excitons and charged trions usually dominate the photoluminescence, rather than that of neutral excitons [17]. This means that many-body interactions play a key role in the electron transport and optical leaps in semiconductor materials [42]. As shown in Fig. 2(c), the Raman spectra of WSe_2 samples were measured on GNEC and undeposited GNEC on silicon substrates; and the right side is the state under the microscope. Compared with the Raman spectrum from WSe_2 on SiO_2/Si substrate, two higher peaks of WSe_2/TGNEC at 1359 and 1592 nm are observed, indicating the existence of graphene nanosheets.

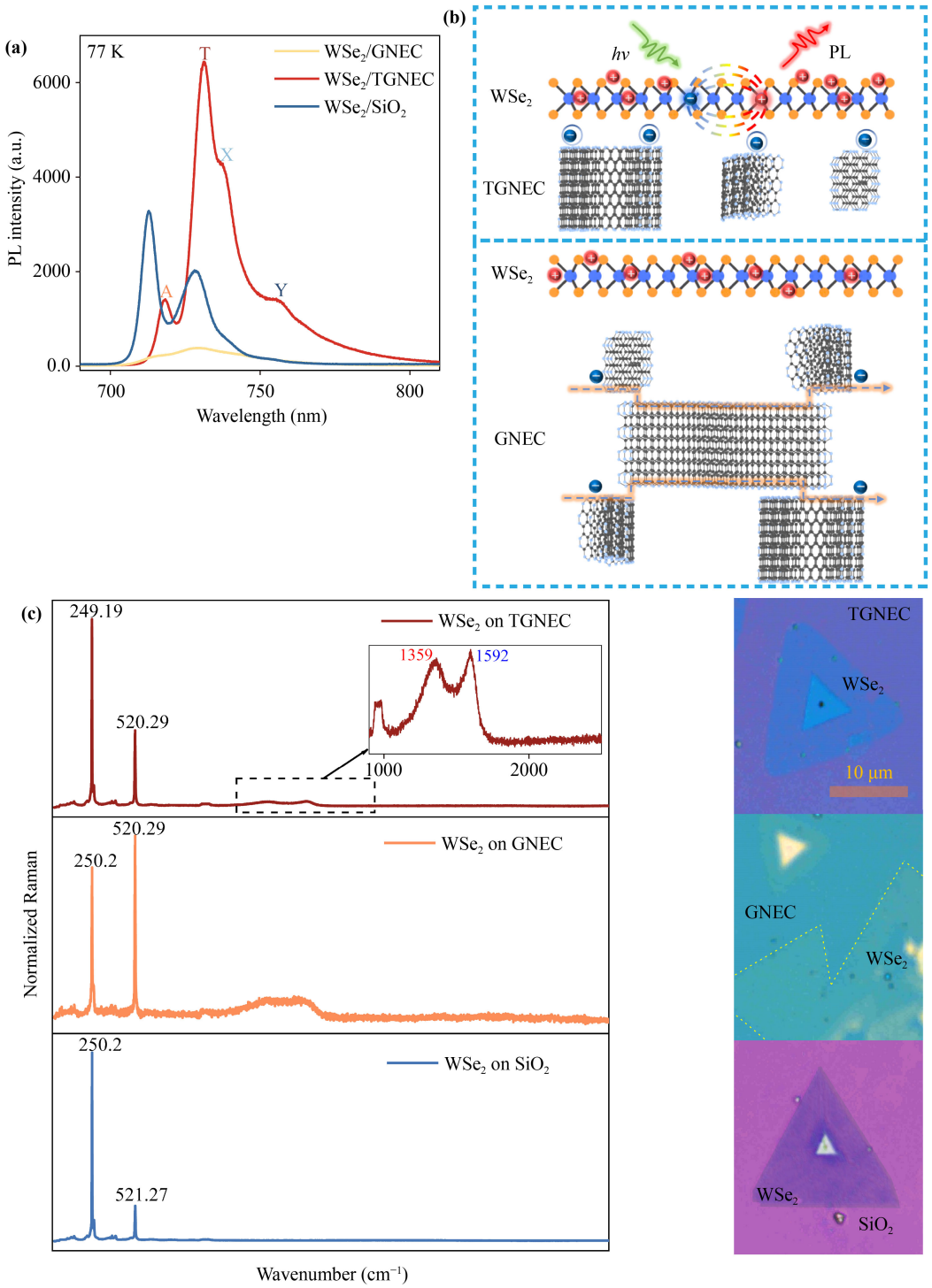

Fig. 2 **(a)** Measured PL spectra from WSe_2/GNEC (purple line), WSe_2/TGNEC (red line) and WSe_2/SiO_2 (blue line) at 77 K. **(b)** Schematic representation of excitons and the electrons trapped by quantum wells (QWs) for TGNEC. The lower part is GNEC's conductive network. **(c)** Measured Raman spectra from WSe_2/TGNEC, WSe_2/GNEC and WSe_2/SiO_2 (blue line). The right side is the state under the microscope.

We performed excitation power-dependent PL measurements at 77 K to further investigate the nature of the observed different multi-exciton peaks. The PL spectra [Fig. 3(a)] were fitted by Gaussian function using three peaks: orange (A peak), yellow (T peak) and blue (X peak). As shown in Fig. 3(a), the purple dashed line is the fit of the Y peak, and the peak width is much larger than the other three peaks. It is caused by defects of substrate, so it has instability. To confirm the designation of each peak, the integrated PL intensities of both the

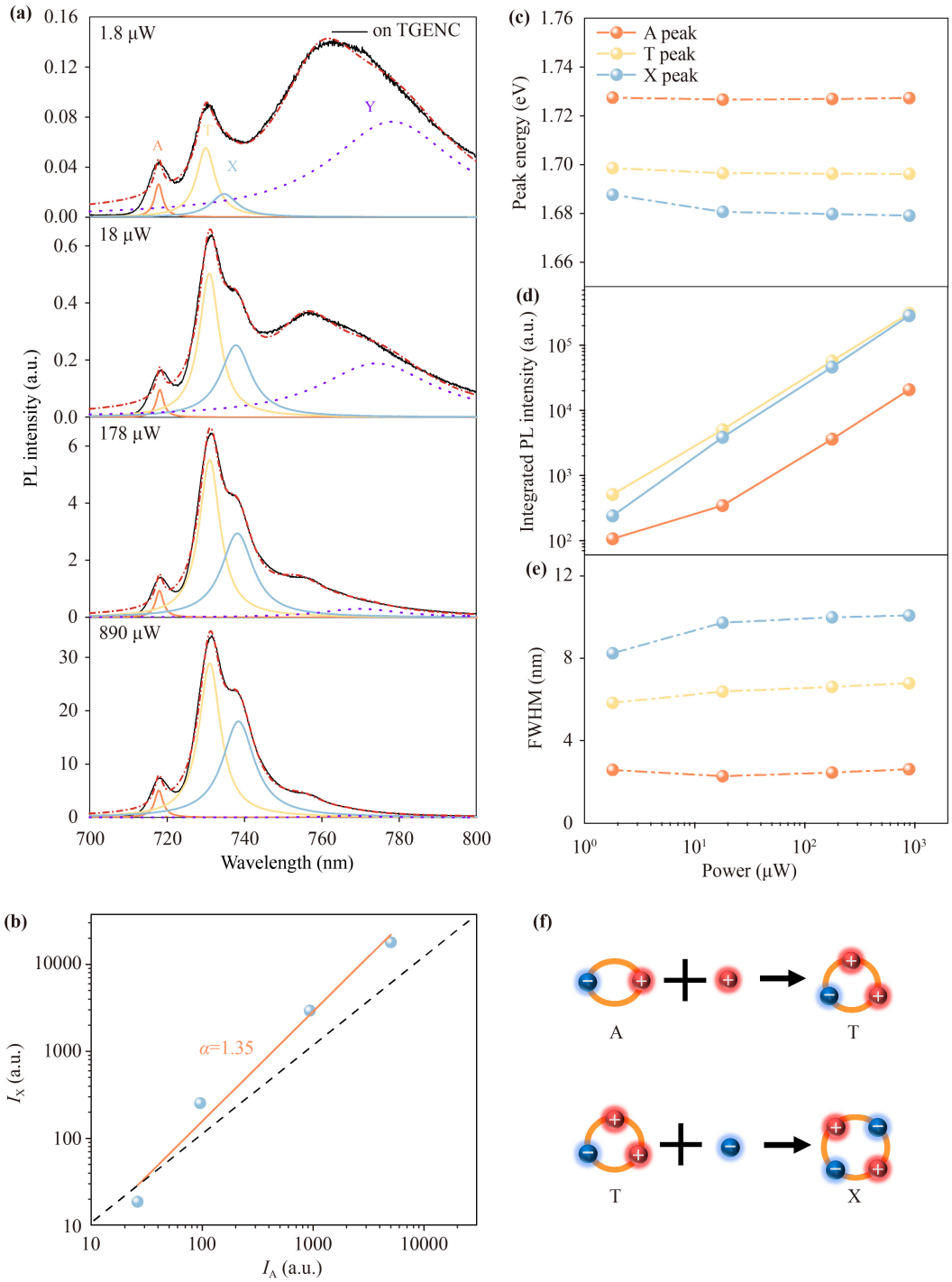

Fig. 3 Power-dependent PL measurements. **(a)** Measured PL spectra from WSe_2/TGNEC at various excitation powers of the 532 nm laser. Spectrum have been fitted by Gaussian function using three peaks: orange (A peak), yellow (T peak) and blue (X peak).Red line shows the cumulative fit. Purple line represents defect peak. **(b)** log–log plot showing the variation of integrated PL intensity of peak X as a function of peak A. From the fitting curve (orange solid line) the PL intensity of peak X grows superlinearly ($\alpha \approx 1.35$), with the increase of the excitation power. **(c)** Variation of A, T and X peak positions with the increase in laser power. **(d)** Integrated PL intensity values plotted with the increase in laser power. **(e)** Full width at half maximum (FWHM) variation with laser power. **(f)** Representative formation of a trion (T) and neutral biexciton (X).

peaks were plotted with respect to each other on a log–log scale [Fig. 3(b)]; the line is fitted by a power-law relation of the form $I_X \propto {I_A}^{\alpha}$, where I_X is the integrated PL intensity of X peak and I_A is the integrated PL intensity of A peak, it is found that peak X grows super linearly with the excitation power ($\alpha \approx 1.35$). In the

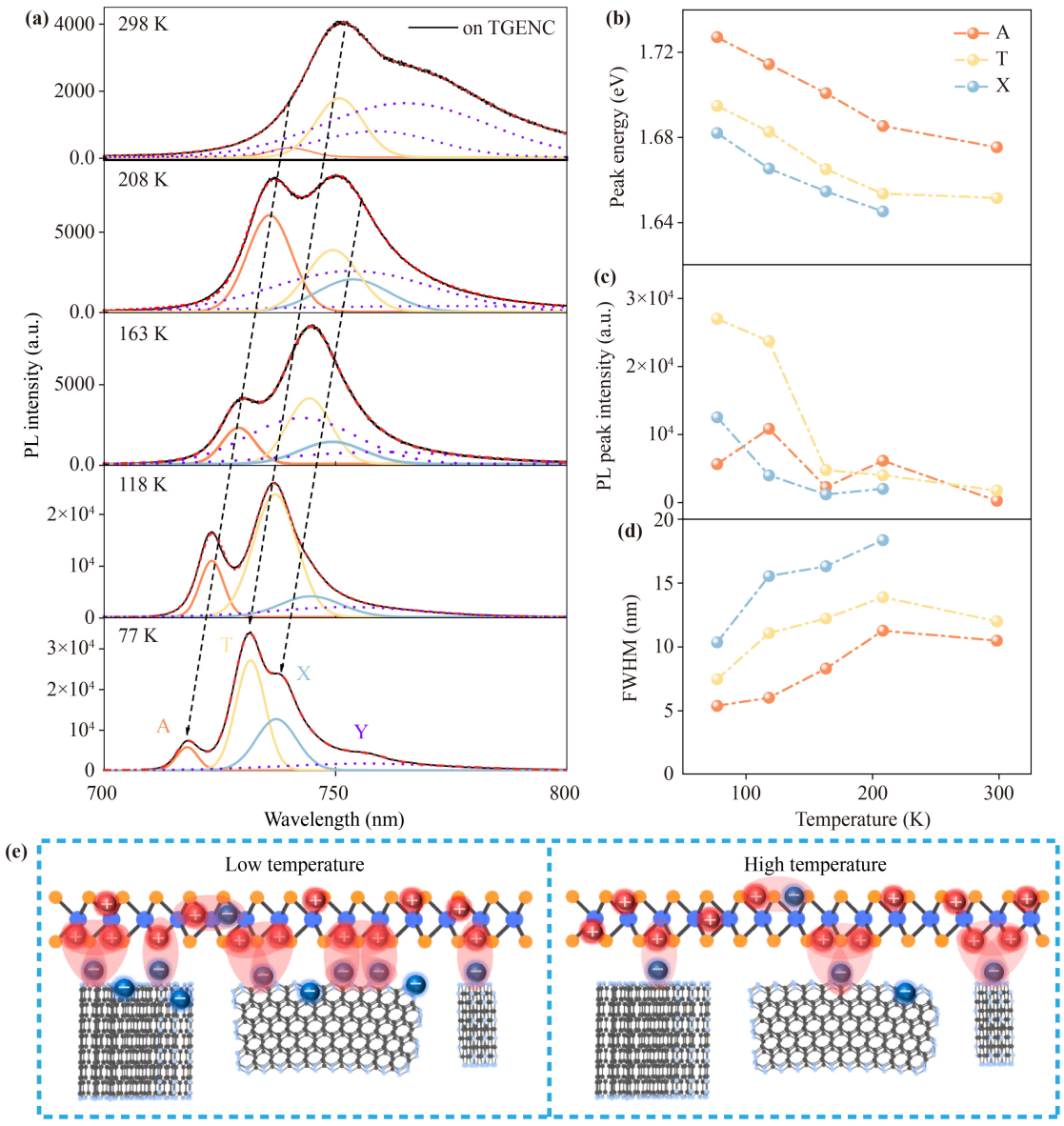

Fig. 4 Temperature-dependent PL measurements. **(a)** Measured PL spectra at various temperatures for WSe_2/TGNEC. **(b–d)** Measured (b) peak position, (c) peak intensity and (d) FWHM of PL peaks A, T and X as a function of temperature in WSe_2/TGNEC. **(e)** Schematic diagram of exciton b inding at low and high temperatures.

ideal case, the PL emission of the exciton state tends to increase linearly (slope $\alpha \approx 1$), and the value of α for the biexciton emission is expected to be close to 2 [43]. However, the α value of the exciton state in TMDs is generally less than 1, and the α value of the biexciton is usually observed between 1.2 and 1.9 [44, 45]. The observed value is less than 2, which may be due to the lack of thermal equilibrium between the exciton states and the limited density of these multiple excitons [44]. According to the fitted α values, peak A is attributed to exciton emission, peak T is attributed to trion emission, and peak X is attributed to biexciton emission. The shifts of the A and T exciton peak positions are small, while the X peak shows a slight red-shift with increasing excitation intensity [Fig. 3(c)]. Figure 3(d) shows the absolute integral PL values plotted as a function of laser power. The full width at half maxima (FWHM) of the A peak does not change much overall after a slight decrease at increasing power, while the FWHM of the X peak becomes wider and the FWHM of T peak is almost constant [Fig. 3(e)]. Usually, the PL intensity growth rate with excitation power varies for excitons in different states due to its different physical mechanisms [46]. The way of exciton binding or recombination is shown in Fig. 3(f), electrons captured by the GNEC edge leap into WSe_2 under laser excitation; electrons bind tightly with the majority carrier-holes in WSe_2 to form excitons; some of the excitons recombine with active electrons to

form trions.

To study the thermal stability and activation energy of these different states of excitons, we also test the devices under the same excitation conditions for temperature-dependent PL. The PL spectra [Fig. 4(a)] were fitted by Gaussian function using three peaks: orange (A peak), yellow (T peak) and blue (X peak). At room temperature, we can also clearly observe the existence of trions, which is difficult to observe in general TMDs materials; but the X peak is difficult to be observed at room temperature. It may be attributed to the fact that the WSe_2 samples are heavily p-doped, which are more likely to combine with a small number of electrons at room temperature to form trions. As shown in Figs. 4(a) and (b), the peak position appears to be red-shifted with increasing temperature. When the temperature rises, the peaks of the excitons in all three states begin to decrease to different degrees. The PL intensity of the T and X peaks decreases sharply with increasing temperature [Fig. 4(c)], indicating that the charged exciton is greatly affected by temperature. Our experimental results are in agreement with the monotonic decrease in exciton emission intensity with increasing temperature as expected by other groups [47–49]. The intensity of PL decreases with increasing temperature because the exciton is not tightly bound to the electron in the edge trap [50]. This weaker mutual bonding is easily affected by temperature changes. With decreasing temperature, the peaks of A, T and X all increase significantly, meaning that more exciton complexes form or recombine in WSe_2. The low temperature leads to a lack of thermal energy for the electrons, so the edge defects of the GNEC trap a large number of electrons [Fig. 4(e)]. It allows free excitons in the two-dimensional space of WSe_2 to locate/capture and radiate recombination, and then emit photons near 750 nm [51]. With increasing temperature, the thermal energy starts to increase and the electrons gain enough energy to avoid the edge trap [Fig. 4(e)]. The electron density at the edge of the carbon film starts to gradually decrease. However, the presence of T peaks can still be clearly observed at room temperature; it indicates that the edge trap of TGNEC has excellent electron trapping ability. The FWHM of the A, T and X peaks generally increase with increasing temperature [Fig. 4(d)]; the FWHM of the A and T peak decreases and then increases at 208 K, which may be caused by the internal defects of WSe_2. In conclusion, due to the increased probability of collision of excitons with longitudinal optical phonons, the exciton values in different states are red-shifted with increasing temperature, and the FWHM becomes wider with increasing temperature [51].

Table 1 Comparison of experimental and theoretical TMD excitonic binding energies (meV)[a].

	System	WSe_2
Experiment	T	30 [41, 42], 31.15[b]
Theory	T	30 [43]
Experiment	X	52 [35], 48.22[b]
Theory	X	59 [43]

[a] Note: A is an exciton, T is a trion, X is a biexciton. [b] This work.

In order to explore the binding energies of different states of excitons and to confirm the correct designation of each peak, we calculated the charged trions binding energy (≈ 31.15 meV) and the neutral biexcitons binding energy (≈ 48.22 meV) at 77 K (see Table 1), which is consistent with the trions binding energy of 30 meV [52, 56] and biexcitons energy of 50–70 meV [43, 45, 55] in the monolayer TMDs. The biexciton binding energy is subtracted by the energy value between the exciton and the biexciton peak; it is assumed that the exciton is generated in the radiation decay of the biexciton [55]. The value of biexcitons binding energy (≈ 49.2 meV) for the former exceeds that found in III–V quantum wells by almost two orders of magnitude [57]. Once again, it shows that we are correct in distinguishing the three characteristic peaks of PL. The biexcitons have a large binding energy, and the trions binding energy is much smaller than the observed biexcitons binding energy. In the supporting information, we measured the binding energies of trion and biexciton at different temperatures and excitation powers. The binding energies were found to be in the range of 24–36 meV for trions and 40–50 meV for biexcitons. The trions binding energy was found to be relatively stable with a small range of variation, while the biexcitons binding energy is more susceptible to the effects of temperature and laser power.

4 Conclusions

In conclusion, we introduced edge quantum wells (QWs) as electron capture centers through GNEC films. It allows free excitons in the two-dimensional space of WSe_2 to locate/capture and radiate recombination. In monolayer WSe_2/TGNEC we observed a strong photoluminescence peak (≈ 730 nm) from trions, and the PL intensity is significantly enhanced. We also performed photoluminescence measurements related to the incident power to confirm the emission characteristics of different exciton states. Meanwhile, we found that these many-body excitons have a high binding energy (charged trions ≈ 31.15 meV, neutral biexcitons ≈ 48.22 meV), which is consistent with experimental results of other subject groups, further indicating that we are correct in distinguishing the exciton states of each peak. Temperature-dependent PL measurements were also performed to explore the thermal stability of excitons in different bound states with increasing temperature. The geometric limits of monolayer TMDs cause enhanced Coulomb interactions and modulate the many-body exciton states of monolayer TMDs through GNEC edge traps, thereby

achieving enhanced optical properties and modulation of carrier transport properties. The introduction of carbon nanofilms to regulate the formation and recombination of exciton complexes, it provides a new idea in the field of studying optoelectronic devices of two-dimensional semiconductors.

Electronic supplementary material Supplementary materials are available in the online version of this article at https://doi.org/10.1007/s11467-022-1232-8 and https://journal.hep.com.cn/fop/EN/10.1007/s11467-022-1232-8.

Acknowledgements The authors gratefully acknowledge the financial support from the National Natural Science Foundation of China (Nos. 62104155, 52275565, 52005343, and 62204117) of China, the Natural Science Foundation of Guangdong Province (No. 2022A1515011667), and the financial support from Jiangsu Province Science Foundation for Youths (No. BK20210275), and Guangdong Kangyi Special Fund (No. 2020KZDZX1173). The authors wish to acknowledge the assistance on TEM/FIB received from the Electron Microscope Center of the Shenzhen University.

References

1. K. S. Novoselov, A. K. Geim, S. V. Morozov, D. Jiang, Y. Zhang, S. V. Dubonos, I. V. Grigorieva, and A. A. Firsov, Electric field effect in atomically thin carbon films, *Science* 306(5696), 666 (2004)
2. S. V. Morozov, K. S. Novoselov, M. I. Katsnelson, F. Schedin, D. C. Elias, J. A. Jaszczak, and A. K. Geim, Giant intrinsic carrier mobilities in graphene and its bilayer, *Phys. Rev. Lett.* 100(1), 016602 (2008)
3. J. W. You, S. R. Bongu, Q. Bao, and N. C. Panoiu, Nonlinear optical properties and applications of 2D materials: Theoretical and experimental aspects, *Nanophoton.* 8, 63 (2018)
4. D. Akinwande, C. J. Brennan, J. S. Bunch, P. Egberts, J. R. Felts, H. Gao, R. Huang, J. S. Kim, T. Li, Y. Li, K. M. Liechti, N. Lu, H. S. Park, E. J. Reed, P. Wang, B. I. Yakobson, T. Zhang, Y. W. Zhang, Y. Zhou, and Y. Zhu, A review on mechanics and mechanical properties of 2D materials — Graphene and beyond, *Extreme Mech. Lett.* 13, 42 (2017)
5. X. Duan, C. Wang, J. C. Shaw, R. Cheng, Y. Chen, H. Li, X. Wu, Y. Tang, Q. Zhang, A. Pan, J. Jiang, R. Yu, Y. Huang, and X. Duan, Lateral epitaxial growth of two-dimensional layered semiconductor heterojunctions, *Nat. Nanotech.* 9(12), 1024 (2014)
6. H. Zeng, J. Dai, W. Yao, D. Xiao, and X. Cui, Valley polarization in MoS_2 monolayers by optical pumping, *Nat. Nanotech.* 7(8), 490 (2012)
7. B. Radisavljevic, A. Radenovic, J. Brivio, V. Giacometti, and A. Kis, Single-layer MoS_2 transistors, *Nature Nanotechno.* 6(3), 147 (2011)
8. S. Bertolazzi, J. Brivio, and A. Kis, Stretching and breaking of ultrathin MoS_2, *ACS Nano* 5(12), 9703 (2011)
9. K. F. Mak, J. Shan, Photonics and optoelectronics of 2D semiconductor transition metal dichalcogenides, *Nat. Photon.* 10(4), 216 (2016)
10. R. Yang, J. Fan, and M. Sun, Transition metal dichalcogenides (TMDCs) heterostructures: Optoelectric properties, *Front. Phys.* 17(4), 43202 (2022)
11. M. Cheng, J. Yang, X. Li, H. Li, R. Du, J. Shi, and J. He, Improving the device performances of two-dimensional semiconducting transition metal dichalcogenides: Three strategies, *Front. Phys.* 17(6), 63601 (2022)
12. Y. Han, J. Yuan, Y. Zhu, Q. Wang, L. Li, and M. Cao, Implantation of WSe_2 nanosheets into multi-walled carbon nanotubes for enhanced microwave absorption, *J. Colloid Interface Sci.* 609, 746 (2022)
13. A. Xie, M. X. Sun, K. Zhang, W. C. Jiang, F. Wu, and M. He, *In situ* growth of MoS_2 nanosheets on reduced graphene oxide (RGO) surfaces: Interfacial enhancement of absorbing performance against electromagnetic pollution, *Phys. Chem. Chem. Phys.* 18(36), 24931 (2016)
14. J. Yang, J. Wang, H. Li, Z. Wu, Y. Xing, Y. Chen, and L. Liu, MoS_2 /MXene aerogel with conformal heterogeneous interfaces tailored by atomic layer deposition for tunable microwave absorption, *Adv. Sci. (Weinh)* 9(7), e2101988 (2022)
15. Q. Q. Wang, B. Niu, Y. H. Han, Q. Zheng, L. Li, and M. S. Cao, Nature-inspired 3D hierarchical structured "vine" for efficient microwave attenuation and electromagnetic energy conversion device, *Chem. Eng. J* 452, 139042 (2023)
16. M. Tosun, L. Chan, M. Amani, T. Roy, G. H. Ahn, P. Taheri, C. Carraro, J. W. Ager, R. Maboudian, and A. Javey, Air-stable n-doping of WSe_2 by anion vacancy formation with mild plasma treatment, *ACS Nano* 10(7), 6853 (2016)
17. C. B. Qin, X. L. Liang, S. P. Han, G. F. Zhang, R. Y. Chen, J. Y. Hu, L. T. Xiao, and S. T. Jia, Giant enhancement of photoluminescence emission in monolayer WS_2 by femtosecond laser irradiation, *Front. Phys.* 16(1), 12501 (2020)
18. Y. Liu, Y. Zhou, H. Zhang, F. Ran, W. Zhao, L. Wang, C. Pei, J. Zhang, X. Huang, and H. Li, Probing interlayer interactions in WSe_2-graphene heterostructures by ultralow-frequency Raman spectroscopy, *Front. Phys.* 14(1), 13607 (2019)
19. B. Wen, Y. Zhu, D. Yudistira, A. Boes, L. L. Zhang, T. Yidirim, B. Q. Liu, H. Yan, X. Q. Sun, Y. Zhou, Y. Z. Xue, Y. P. Zhang, L. Fu, A. Mitchell, H. Zhang, and Y. Lu, Ferroelectric-driven exciton and trion modulation in monolayer molybdenum and tungsten diselenides, *ACS Nano* 13(5), 5335 (2019)
20. S. Imani Yengejeh, W. Wen, and Y. Wang, Mechanical properties of lateral transition metal dichalcogenide heterostructures, *Front. Phys.* 16(1), 13502 (2020)
21. Y. Yang, Z. W. Jie, Z. W. Ying, L. Xian, J. Z. Ming, L. W. Min, and M. G. Hong, Dynamics of A-exciton and spin relaxation in WS_2 and WSe_2 monolayer, *Acta Phys. Sin.* 68(1), 017201 (2019) (in Chinese)

22. V. Shahnazaryan, I. Iorsh, I. A. Shelykh, and O. Kyrienko, Exciton–exciton interaction in transition-metal dichalcogenide monolayers, *Phys. Rev. B* 96(11), 115409 (2017)
23. K. F. Mak, K. He, C. Lee, G. H. Lee, J. Hone, T. F. Heinz, and J. Shan, Tightly bound trions in monolayer MoS_2, *Nat. Mater.* 12(3), 207 (2013)
24. Z. P. Li, T. M. Wang, Z. G. Lu, C. H. Jin, Y. W. Chen, Y. Z. Meng, Z. Lian, T. Taniguchi, K. Watanabe, S. Zhang, D. Smirnov, and S.-F. Shi, Revealing the biexciton and trion-exciton complexes in BN encapsulated WSe_2, *Nat. Commun.* 9(1), 3719 (2018)
25. E. J. Sie, A. J. Frenzel, Y.-H. Lee, J. Kong, and N. Gedik, Intervalley biexcitons and many-body effects in monolayer MoS_2, *Phys. Rev. B* 92(12), 125417 (2015)
26. K. Hao, J. F. Specht, P. Nagler, L. Xu, K. Tran, A. Singh, C. K. Dass, C. Schüller, T. Korn, M. Richter, A. Knorr, X. Li, and G. Moody, Neutral and charged intervalley biexcitons in monolayer $MoSe_2$, *Nat. Commun.* 8(1), 15552 (2017)
27. J. S. Ross, S. Wu, H. Yu, N. J. Ghimire, A. M. Jones, G. Aivazian, J. Yan, D. G. Mandrus, D. Xiao, W. Yao, and X. Xu, Electrical control of neutral and charged excitons in a monolayer semiconductor, *Nat. Commun.* 4, 1474 (2013)
28. A. Ramasubramaniam, Large excitonic effects in monolayers of molybdenum and tungsten dichalcogenides, *Phys. Rev. B* 86(11), 115409 (2012)
29. R. C. Miller, D. A. Kleinman, W. T. Tsang, and A. C. Gossard, Observation of the excited level of excitons in GaAs quantum wells, *Phys. Rev. B* 24(2), 1134 (1981)
30. R. L. Greene, K. K. Bajaj, and D. E. Phelps, Energy levels of Wannier excitons in GaAs–$Ga_{1-x}Al_xAs$ quantum-well structures, *Phys. Rev. B* 29(4), 1807 (1984)
31. K. L. He, N. Kumar, L. Zhao, Z. F. Wang, K. F. Mak, H. Zhao, and J. Shan, Tightly bound excitons in monolayer WSe_2, *Phys. Rev. Lett.* 113(2), 026803 (2014)
32. H. Q. Ying and X. Yang, Detection of dielectric screening effect by excitons in two-dimensional semiconductors and its application, *Acta Phys. Sin.* 71(12), 127102 (2022) (in Chinese)
33. C. Wang, X. Zhang, and D. Diao, Nanosized graphene crystallite induced strong magnetism in pure carbon films, *Nanoscale* 7(10), 4475 (2015)
34. W. C. Chen, X. Zhang, and D. F. Diao, Low-energy electron excitation effect on formation of graphene nanocrystallites during carbon film growth process, *Appl. Phys. Lett.* 111, 114105 (2017)
35. X. Zhang, Z. Lin, D. Peng, and D. Diao, Bias-modulated high photoelectric response of graphene-nanocrystallite embedded carbon film coated on n-silicon, *Nanomaterials* 9(3) (2019)
36. S. Devaraj and N. Munichandraiah, Effect of crystallographic structure of MnO_2 on its electrochemical capacitance properties, *J. Phys. Chem. C* 112(11), 4406 (2008)
37. S. J. Yoo, C. Y. Kim, J. W. Shin, S. G. Lee, J. M. Jeong, Y. J. Kim, S. H. Lee, and J. G. Kim, Characterization of an amorphous carbon film covering a Mo grid during *in situ* heating TEM study, *Mater. Charact.* 78, 31 (2013)
38. S. Y. Gao, L. Liu, Z. Z. Lin, X. Zhang, and D. F. Diao, High photoresponsivity of vertical graphene nanosheets/P-Si enhanced by electron trapping at edge quantum wells, *J. Phys. Chem. C* 125(9), 5392 (2021)
39. M. D. Tran, J. H. Kim, and Y. H. Lee, Tailoring photoluminescence of monolayer transition metal dichalcogenides, *Curr. Appl. Phys.* 16(9), 1159 (2016)
40. J. Yang, T. Y. Lü, Y. W. Myint, J. J. Pei, D. Macdonald, J. C. Zheng, and Y. R. Lu, Robust excitons and trions in monolayer $MoTe_2$, *ACS Nano* 9(6), 6603 (2015)
41. B. Zhu, X. Chen, and X. Cui, Exciton binding energy of monolayer WS_2, *Sci. Rep.* 5, 9218 (2015)
42. Z. Z. Yan, Z. H. Jiang, J. P. Lu, and Z. H. Ni, Interfacial charge transfer in WS_2 monolayer/$CsPbBr_3$ microplate heterostructure, *Front. Phys.* 13(4), 138115 (2018)
43. J. Pei, J. Yang, X. Wang, F. Wang, S. Mokkapati, T. Lü, J. C. Zheng, Q. Qin, D. Neshev, H. H. Tan, C. Jagadish, and Y. Lu, Excited state biexcitons in atomically thin $MoSe_2$, *ACS Nano* 11(7), 7468 (2017)
44. Y. M. You, X. X. Zhang, T. C. Berkelbach, M. S. Hybertsen, D. R. Reichman, and T. F. Heinz, Observation of biexcitons in monolayer WSe_2, *Nat. Phys.* 11(6), 477 (2015)
45. J. Z. Shang, X. N. Shen, C. X. Cong, N. Peimyoo, B. C. Cao, M. Eginligil, and T. Yu, Observation of excitonic fine structure in a 2D transition-metal dichalcogenide semiconductor, *ACS Nano* 9(1), 647 (2015)
46. M. Tebyetekerwa, J. Zhang, Z. Xu, T. N. Truong, Z. Yin, Y. Lu, S. Ramakrishna, D. Macdonald, and H. T. Nguyen, Mechanisms and applications of steady-state photoluminescence spectroscopy in two-dimensional transition-metal dichalcogenides, *ACS Nano* 14(11), 14579 (2020)
47. A. T. Hanbicki, G. Kioseoglou, M. Currie, C. S. Hellberg, K. M. McCreary, A. L. Friedman, and B. T. Jonker, Anomalous temperature-dependent spin-valley polarization in monolayer WS_2, *Sci. Rep.* 6, 18885 (2016)
48. J. M. Li, X. Yuan, P. T. Jing, J. Li, M. B. Wei, J. Hua, J. L. Zhao, and L. H. Tian, Temperature-dependent photoluminescence of inorganic perovskite nanocrystal films, *RSC Adv.* 6(82), 78311 (2016)
49. T. Kato and T. Kaneko, Optical detection of a highly localized impurity state in monolayer tungsten disulfide, *ACS Nano* 8(12), 12777 (2014)
50. Z. W. Wang, R. Z. Li, X. Y. Dong, Y. Xiao, and Z. Q. Li, Temperature dependence of the excitonic spectra of monolayer transition metal dichalcogenides, *Front. Phys.* 13(4), 137305 (2018)
51. A. Sharma, B. Wen, B. Q. Liu, Y. W. Myint, H. Zhang, and Y. Lu, Defect engineering in few-layer phosphorene, *Small* 14(16), 1704556 (2018)
52. A. M. Jones, H. Y. Yu, N. J. Ghimire, S. F. Wu, G. Aivazian, J. S. Ross, B. Zhao, J. Q. Yan, D. G. Mandrus, D. Xiao, W. Yao, and X. D. Xu, Optical

generation of excitonic valley coherence in monolayer WSe_2, *Nat. Nanotech.* 8(9), 634 (2013)

53. G. Wang, L. Bouet, D. Lagarde, M. Vidal, A. Balocchi, T. Amand, X. Marie, B. Urbaszek, Valley dynamics probed through charged and neutral exciton emission in monolayer WSe_2, *Phys. Rev. B* 90(7), 075413 (2014)
54. D. K. Zhang, D. W. Kidd, and K. Varga, Excited biexcitons in transition metal dichalcogenides, *Nano Lett.* 15(10), 7002 (2015)
55. Y. You, X.-X. Zhang, T. C. Berkelbach, M. S. Hybertsen, D. R. Reichman, and T. F. Heinz, Observation of biexcitons in monolayer WSe_2, *Nat. Phys.* 11(6), 477 (2015)
56. G. Wang, X. Marie, I. Gerber, T. Amand, D. Lagarde, L. Bouet, M. Vidal, A. Balocchi, and B. Urbaszek, Giant enhancement of the optical second-harmonic emission of WSe_2 monolayers by laser excitation at exciton resonances, *Phys. Rev. Lett.* 114(9), 097403 (2015)
57. C. F. Klingshirn, *Semiconductor Optics*, Ed. 3, Springer-Verlag Berlin, Heidelberg, 2007 doi: 10.1007/978-3-540-38347-5